Self-Assembly

International Edition: DOI: 10.1002/anie.201900428
German Edition: DOI: 10.1002/ange.201900428

Modular Design of Noble-Metal-Free Mixed Metal Oxide Electrocatalysts for Complete Water Splitting

Dandan Gao, Rongji Liu, Johannes Biskupek, Ute Kaiser, Yu-Fei Song, and Carsten Streb**

Abstract: *Electrocatalytic water splitting into H_2 and O_2 is a key technology for carbon-neutral energy. Here, we report a modular materials design leading to noble metal-free composite electrocatalysts, which combine high electrical conductivity, high OER and HER reactivity and high durability. The scalable bottom-up fabrication allows the stable deposition of mixed metal oxide nanostructures with different functionalities on copper foam electrodes. The composite catalyst shows sustained OER and HER activity in 0.1 M aqueous KOH over prolonged periods ($t > 10$ h) at low overpotentials (OER: ≈ 300 mV; HER: ≈ 100 mV) and high faradaic efficiencies (OER: ≈ 100 %, HER: ≈ 98 %). The new synthetic concept will enable the development of multifunctional, mixed metal oxide composites as high-performance electrocatalysts for challenging energy conversion and storage reactions.*

Electrocatalytic water splitting into hydrogen and oxygen is one of the most promising catalytic approaches for carbon-neutral energy storage.[1–3] The overall process is based on two coupled electrochemical half-reactions, the oxygen evolution reaction (OER)[4,5] and the hydrogen evolution reaction (HER).[2,6,7] For industrial relevance, both half-reactions require noble-metal-free catalysts, which combine high activity with long-term stability. Therefore, synthetic methods are required for the chemically, mechanically and electrically stable anchoring of high-performance catalysts on conductive electrode surfaces.[1,2,8] State-of-the-art electrocatalysis research has been focused on the independent development of HER and OER catalysts, so that each half-reaction can be individually optimized.[1–3] For HER electrocatalysis,[9] the focus has been on homo- or heterometallic transition metal oxides,[10] sulfides,[11] nitrides,[12] carbides,[12] and phosphides.[13] For OER,[5] the leading electrocatalysts are homo- and heterometallic transition metal oxides,[14,15] hydroxides,[16,17] phosphates,[18] and nitrides.[19] In contrast, the design of bifunctional catalysts capable of OER and HER electrocatalysis is still in its infancy and faces major challenges, as new catalysts are needed, which feature the redox-chemistries, stabilities and catalytic capabilities for reductive and oxidative proton-coupled electron transfers. However, the design of bifunctional OER/HER electrocatalysts offers vast advantages as it would simplify catalyst design and fabrication, prevent cross-contamination, materials incompatibilities and possible catalyst poisoning and is therefore of enormous technological interest. In addition, HER and OER electrocatalysis share common challenges including the need for high electrical conductivity, the stable catalyst-electrode anchoring and others, so that a convergent OER/HER catalyst design could overcome major current obstacles in electrocatalysis. To date, only few materials have shown this broad range of properties and most pioneering studies have used metal phosphides such as nickel phosphides,[20] iron nickel phosphides,[6] and nickel cobalt phosphides[21] or nickel selenide nanosheets.[22] In contrast, less research has been devoted to bifunctional metal oxides for complete water-splitting, although ground-breaking studies have explored copper cobalt oxide nanowires[23] and nickel cobalt oxide nanoflakes[24] on metal electrodes as well as iron nickel oxide nanoparticles on carbon nanofibers[25] for OER/HER electrocatalysis.

Here we report a modular design approach where several metal oxide components are rationally targeted to introduce electrical conductivity, OER/HER catalytic activity and structural stability into a composite electrocatalyst. Simultaneous deposition of the mixed metal oxides on metal electrodes is reported and the electrodes are deployed in a 2-electrode water electrolyzer to demonstrate the technological relevance. High operational durability ($t_{electrolysis} > 10$ h), low total overpotential (0.57 V at $J \approx 10$ mA cm^{-2}) and high faradaic efficiencies were observed. Post-catalytic studies highlight the chemical and mechanical stability of the catalyst. This first proof of concept opens the door for designer catalysts where molecular precursors are converted into stable nanostructures for challenging multi-electron electrocatalysis (Figure 1).

[*] M. Sc. D. Gao, Dr. R. Liu, Prof. Dr. C. Streb
Institute of Inorganic Chemistry I, Ulm University
Albert-Einstein-Allee 11, 89081 Ulm (Germany)
E-mail: carsten.streb@uni-ulm.de
Prof. Dr. C. Streb
Helmholtz-Institute Ulm
Helmholtzstrasse 11, 89081 Ulm (Germany)
Dr. R. Liu
Key Laboratory of Green Process and Engineering
Institute of Process Engineering, Chinese Academy of Sciences
100190 Beijing (P. R. China)
Dr. J. Biskupek, Prof. Dr. U. Kaiser
Electron Microscopy of Materials Science
Central Facility for Electron Microscopy, Ulm University
Albert-Einstein-Allee 11, 89081 Ulm (Germany)
Prof. Dr. Y.-F. Song
State Key Laboratory of Chemical Resource Engineering
Beijing University of Chemical Technology
100029 Beijing (P. R. China)
E-mail: songyf@mail.buct.edu.cn
songyufei@hotmail.com
Supporting information and the ORCID identification number(s) for the author(s) of this article can be found under: https://doi.org/10.1002/anie.201900428.

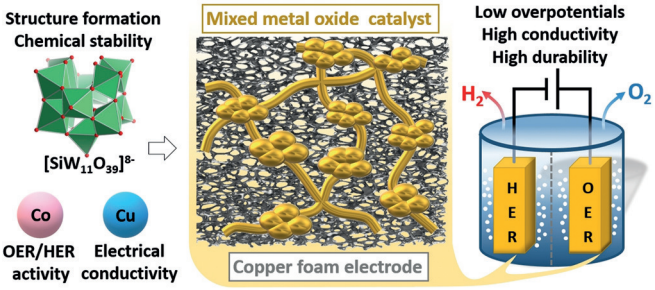

Figure 1. Schematic materials design and fabrication approach leading to mixed metal oxide electrodes. Hydrothermal deposition of cobalt, copper and tungsten oxide precursors on copper foam electrodes gives stable bifunctional electrocatalysts for high-efficiency OER and HER.

Here, we report a bottom-up materials design approach, where metal oxides with different functionality are stably anchored on a metal foam electrode in a scalable one-step synthesis. To this end, we targeted a mixed metal oxide composite featuring cobalt oxides as high-performance OER[26] and HER catalysts,[27] semiconducting copper oxides for enhanced electron transport,[28] and tungsten oxides for structural and chemical stability and electrode durability.[4] Electrode design was based on the use of commercial, macroporous copper foam (**CF**) electrodes, which offer high electrical conductivity, high surface area as well as efficient electrolyte accessibility and gaseous product release.[4]

Functionalization of the **CF** electrodes with the mixed metal oxide catalyst was achieved by hydrothermal reaction of the molecular precursors $Co(NO_3)_2{\cdot}6H_2O$ (1.04 mmol) and $K_8[SiW_{11}O_{39}]{\cdot}13H_2O$ (1.0 mmol) with **CF** (which serves as Cu ion source)[4] at 150 °C for 8 h (details see Supporting Information, Table S1 and Figure S1). The washed and dried samples (hereafter: **Electrode 1**) were examined by gravimetric studies which gave a catalyst loading of ca. 1.25 mg cm^{-2} based on geometric surface area. Powder X-ray diffraction (pXRD, Supporting Information, Figure S8) showed the presence of crystalline Cu_2O, which is a known semiconductor with high electron mobility[28] and has recently been reported as OER and HER catalyst.[23,29–33] Scanning electron microscopy (SEM), energy dispersive X-ray spectroscopy (EDX) and transmission electron microscopy (TEM) showed a homogeneous deposition of spherical nanoparticles (diameter ≈200–600 nm) and high aspect-ratio nanowires (diameter ≈50 nm, length >4 μm, Figure 2 and Figure S6) on the macroporous support. EDX elemental mapping (Figure 2d and Figure S5) showed a homogeneous distribution of the elements Cu, Co, and W on the electrode, and inductively coupled plasma atomic emission spectroscopy gives an atomic ratio of 1:1.5:8 (Co:W:Cu), Table S2. TEM analysis by local selected area electron diffraction (SAED) indicates that the nanowires are based on single crystalline Cu_2O (Figure 2c, Figure S6). Note that analyses were performed on powder material removed from the **CF** electrode by prolonged sonication. The presence of a mixed metal oxide was further supported by FT-IR and Raman spectroscopies, where characteristic vibrational modes were observed, see Figure S9.[34,35] FT-IR spectroscopy also identified the presence of O-H vibrations and thermogravimetric analyses (TGA) indicated the presence of ca. 5.7 wt-% water of hydration, Figure S7.

To assess the role of the metal oxide precursors used in the synthesis, we performed identical syntheses in the absence of Co^{2+}, $[SiW_{11}O_{39}]^{8-}$ and NO_3^-. Note that in the absence of any of the precursors, no nanostructured metal oxide composites were obtained (see Table 1 and Figures S2–S4). The resulting electrodes (**Electrodes 2–4**) were used as references to compare the electrocatalytic performance of **Electrode 1** (Table 1).

Table 1: Comparison of the electrocatalytic OER and HER performance of **Electrode 1** with selected reference systems.

Electrodes	Overpotential[a] [mV]		Tafel slopes [mV dec^{-1}]		ECSA [cm^2]	R_{ct} [Ω]
	OER	HER	OER	HER		
Electrode 1	313	−103	162 ± 0.7	335 ± 1.0	275 ± 7	13.0
References[b]						
Electrode 2	420	−192	187 ± 3.0	318 ± 5.0	85 ± 7	32.8
Electrode 3	480	−421	144 ± 1.0	793 ± 10	25 ± 2	29.0
Electrode 4	470	−440	123 ± 0.4	274 ± 2.0	20 ± 2	29.0
CF	500	−456	119 ± 0.2	154 ± 0.5	–	29.0

[a] $J = 10$ mA cm^{-2}, [b] **Electrodes 2–4** were prepared by the original synthetic procedure in the absence of $[SiW_{11}O_{39}]^{8-}$ (**2**), Co^{2+}/NO_3^- (**3**) or Co^{2+} (**4**), detailed characterization see Supporting Information.

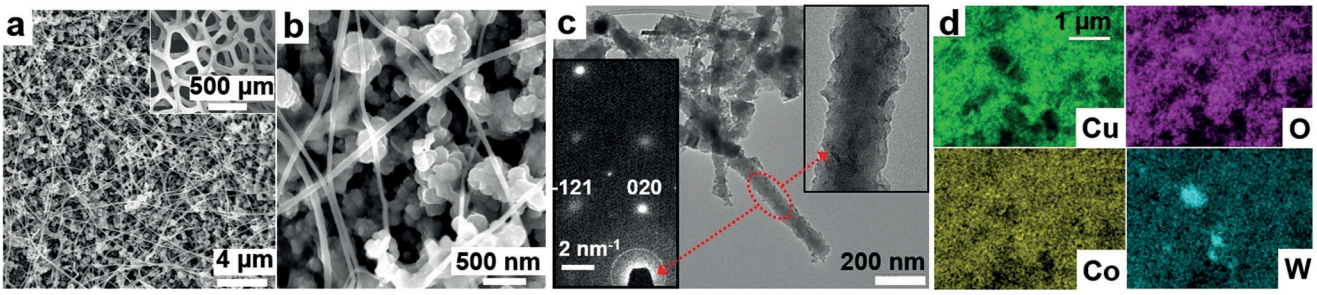

Figure 2. Structural and chemical characterization of the nanostructured composite. a) SEM survey image of **Electrode 1** (Inset: low magnification view of the macroporous electrode structure); b) High resolution SEM image of the spherical and nanowire Co-Cu-W oxide catalyst; c) TEM image of nanowires and particles; inset (left): selected area electron diffraction of the nanowire showing diffraction spots matching reflections of Cu_2O in [101] zone axis orientation; inset (right): magnified image of the Cu_2O nanowire; d) EDX elemental mapping of **Electrode 1** showing the distribution of the elements Cu, Co, W, and O.

X-ray photoelectron spectroscopy (XPS) was used to gain insight into the chemical nature of the metal species and confirmed the presence of Co^{2+}, $Cu^{+/2+}$, and W^{6+} (Figure 3 and Figure S8). The observation of Cu^{+} and Cu^{2+} could

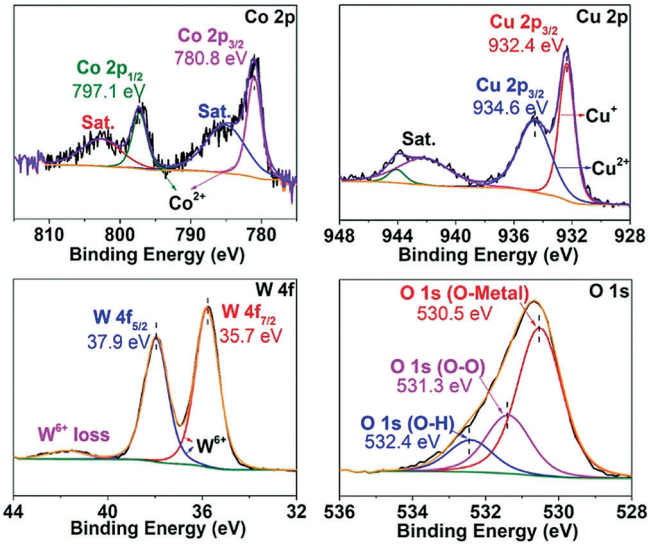

Figure 3. Deconvoluted XPS spectra of the mixed metal oxide catalyst recovered from **Electrode 1**. Recovery of the metal oxide composites from the electrode was achieved by prolonged sonication in ethanol.

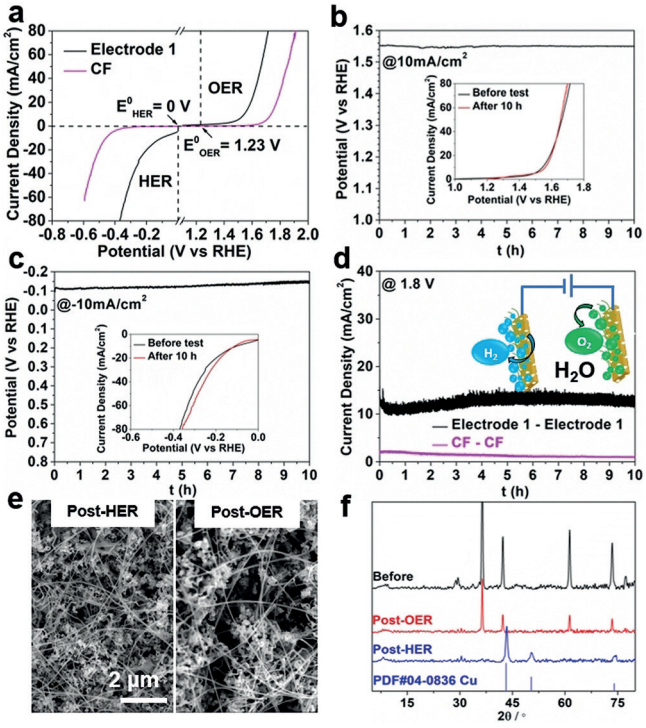

Figure 4. Catalytic performance of **Electrode 1** for OER, HER and full water splitting. a) LSV polarization curves of **Electrode 1** and the non-modified **CF** reference in 0.1 M aqueous KOH, scan rate 5 $mV s^{-1}$, current densities are based on geometric surface area; b) OER and c) HER long-term chronopotentiometry studies of **Electrode 1** at $J = 10\ mA cm^{-2}$; inset: pre- and post-catalytic comparison of OER/HER performance; d) Full electrocatalytic water-splitting by **Electrode 1** at a constant potential of 1.8 V vs. RHE (using a 2-electrode setup). Non-modified **CF** is shown as reference; inset: schematic illustration of the full process. Post-catalytic analyses of **Electrode 1** after OER/ HER using e) SEM and f) pXRD.

indicate two distinct copper-containing phases, for example, Cu_2O and a Cu^{2+}-containing (amorphous) metal oxide. Alternatively, it could indicate the literature-known surface oxidation of Cu_2O to CuO.[36,37] The deconvoluted O1s spectrum indicates the presence of oxygen-metal bonds (O–Co, O–Cu, O–W) and hydroxyl groups (O–H).[37–39] In sum, this materials analysis suggests that a mixed metal oxide phase is present containing crystalline Cu_2O particles together with amorphous, hydrated copper, cobalt and tungsten oxide phases. The exact structural properties of this complex system will be further explored using spectroscopic, magnetometric, diffractometric and theoretical methods in subsequent studies.

In the next step, we examined the electrocatalytic performance of the composite electrode for the OER and HER under conditions typically used in alkaline water electrolysis studies (0.1M aqueous KOH, pH 12.8, RT). All potentials were converted to the reversible hydrogen electrode (RHE) as reference. Linear sweep voltammetric (LSV) polarization curves (Figure 4a) show that **Electrode 1** features excellent catalytic activity for both OER and HER: low overpotentials η (at $J = 10\ mA cm^{-2}$, scan rate $= 5\ mV s^{-1}$) were observed for OER ($\eta = 313$ mV) and HER ($\eta = -103$ mV). In contrast, the non-modified **CF** as well as several reference electrodes modified with Co^{2+} or $[SiW_{11}O_{39}]^{8-}$ showed significantly lower performance and higher overpotentials (Table 1, Figure S10). Next, we assessed the long-term performance of **Electrode 1** for OER and HER by chronopotentiometry ($J = 10\ mA cm^{-2}$) over a period of 10 h. For OER the potential observed remained stable at 1.55 V (Figure 4b). For HER, the initial potential (−0.11 V) changed to −0.14 V after 10 h (Figure 4c), indicating minor structural or chemical changes of the electrode (see below). Comparison of the LSV curves for OER and HER before and after 10 h electrolysis (Insets in Figure 4b, c) show the near-identical performance and provide further support of the high stability of the composite under harsh oxidative and reductive electrocatalytic conditions.

The full water-splitting capabilities of **Electrode 1** were examined by combining two identical **Electrode 1** units in a 2-electrode water electrolyzer using 0.1M aqueous KOH as electrolyte. At an applied potential of 1.8 V ($\eta = 0.57$ V), sustained gas evolution was observed at both electrodes (Figure S12a). Chronoamperometry over 10 h (Figure 4d) show that sustained water-splitting is possible at current densities between $J = 10$–$14\ mA cm^{-2}$. In contrast, identical experiments with two non-modified **CF** electrodes show no gas evolution and current densities of only $\approx 2\ mA cm^{-2}$ (Figure 4d, Figure S12b). High faradaic efficiencies were determined for both OER ($\approx 100\%$) and HER ($\approx 98\%$), highlighting the efficient electrochemical processes for OER and HER catalyzed by the mixed-metal composite catalyst, see Figure S13.

Post-catalytic analyses of the OER and HER electrodes were performed after 10 h sustained electrolysis. SEM data show that the morphology and shape of the nanostructured particles on the electrode are not altered (Figure 4e). This is further supported by SEM-EDX elemental mapping after catalysis which shows the homogeneous distribution of the metal components on the electrode surface (Figures S14, S15). pXRD and post-catalytic XPS analyses after OER show no significant crystallographic or elemental changes (Figure 4f and Figure S16). In contrast, after HER, the original diffraction signals for Cu_2O disappear and new signals are observed, which are indexed as elemental Cu (Figure 4f). Post-HER-catalytic XPS analyses (Figure S17) indicate the presence of Cu^0 and Cu^{2+} but show no Cu^+. In sum we conclude that under HER catalytic conditions Cu^+ is reduced to elemental Cu, while Cu^{2+} is still present. This is in line with the experimental HER studies where we note a slight change of the HER potential (from −0.11 V to −0.14 V during 10 h electrolysis) which also indicates a slow chemical change of the electrode. Note that based on all electrochemical data and post-catalytic SEM analyses, this does not affect the performance or stability of the electrode. In addition, no mechanical detachment of the catalyst from the electrode ("flaking") is observed during long-term electrolysis.

To gain mechanistic insights into the high OER and HER performance and high stability of **Electrode 1**, we performed further (electro)chemical analyses. Electrochemical impedance spectroscopy (EIS) showed that **Electrode 1** features a significantly lower charge transfer resistance (R_{ct}) compared to all references studied (Table 1, Figure S18). This highlights the superior conductivity between the copper foam support and the mixed metal oxide catalyst, which enables efficient interfacial electron transport, even in the absence of a binder or conductive additive (e.g., conductive carbon). In addition, the long-term electrolytic studies (Figure 4b–d) highlight the robust anchoring of the catalyst on the electrode surface, which results in high operational durability. The role of the nanostructured electrode surface was examined by electrochemical surface area analyses (ECSA) and hydrophilicity studies: ECSA analyses based on cyclic voltammetry of **Electrode 1** showed high ECSA values ($>270\ cm^2$) which is significantly higher than any of the references studied (≈ 20–$80\ cm^2$) (Table 1, Figure S19). The combination of macroporous metal support, nanostructured catalyst surface and high ECSA enable high catalytic turnover rates and allow the facile release of the gaseous products from the electrode (thus preventing bubble overpotentials and efficiency-limiting high current densities).[40] Analysis of the hydrophilicity of the electrode surfaces by the sessile drop method (using 0.1M aqueous KOH as medium) showed that **Electrode 1** is highly wettable and a drop deposited on the electrode surface permeates into the macroporous structure within two seconds. In contrast, the native **CF** electrode shows a significantly lower wettability and a deposited drop remains on the electrode surface and shows a contact angle of 69° (Figure S20). The formation of a stable electrolyte-catalyst interface is therefore enabled by the hydrophilic nanostructure surface of **Electrode 1**.

In conclusion, we report a modular, scalable route for the simultaneous deposition of several nanostructured mixed metal oxides on metal foam electrodes. The resulting composite is used as a bifunctional electrocatalyst for sustained full water splitting into H_2 and O_2 under conditions used in alkaline water electrolyzers. Low overpotentials, high faradaic efficiencies and long operational times without loss of reactivity are observed. We propose that this new materials design concept enables the targeted development of complex multicomponent composite catalysts and their simultaneous electrical wiring to conductive electrode surfaces. The study could therefore provide a protocol for novel mixed-metal oxides as (electro-)catalysts for challenging multielectron transfer reactions.

Acknowledgements

This research was supported by China Scholarship Council, Ulm University and the Deutsche Forschungsgemeinschaft DFG (TRR234, CataLight, projects B3 and C4). R.L. acknowledges the Alexander-von-Humboldt-Foundation for a postdoctoral fellowship. Y.-F.S. acknowledges the National Natural Science Foundation of China. M.Sc. Hannah Braun, M.Sc. Ruihao Gong, Dr. Thomas Diemant and Prof. Dr. Othmar Marti are acknowledged for experimental support and instrument access.

Conflict of interest

The authors declare no conflict of interest.

Keywords: electrocatalysis · metal Oxide · polyoxometalates · self-assembly · water-splitting

How to cite: *Angew. Chem. Int. Ed.* **2019**, *58*, 4644–4648
Angew. Chem. **2019**, *131*, 4692–4696

[1] I. Roger, M. A. Shipman, M. D. Symes, *Nat. Rev. Chem.* **2017**, *1*, 0003.
[2] C. C. L. McCrory, S. Jung, I. M. Ferrer, S. M. Chatman, J. C. Peters, T. F. Jaramillo, *J. Am. Chem. Soc.* **2015**, *137*, 4347–4357.
[3] P. Du, R. Eisenberg, *Energy Environ. Sci.* **2012**, *5*, 6012.
[4] W. Luo, J. Hu, H. Diao, B. Schwarz, C. Streb, Y.-F. Song, *Angew. Chem. Int. Ed.* **2017**, *56*, 4941–4944; *Angew. Chem.* **2017**, *129*, 5023–5026.
[5] C. C. L. McCrory, S. Jung, J. C. Peters, T. F. Jaramillo, *J. Am. Chem. Soc.* **2013**, *135*, 16977–16987.
[6] F. Yu, H. Zhou, Y. Huang, J. Sun, F. Qin, J. Bao, W. A. Goddard, S. Chen, Z. Ren, *Nat. Commun.* **2018**, *9*, 1–9.
[7] E. S. Andreiadis, P.-A. Jacques, P. D. Tran, A. Leyris, M. Chavarot-Kerlidou, B. Jousselme, M. Matheron, J. Pécaut, S. Palacin, M. Fontecave, V. Artero, *Nat. Chem.* **2012**, *5*, 48–53.
[8] M. Yang, J. Dan, S. J. Pennycook, X. Lu, H. Zhu, Q. Xu, H. J. Fan, G. W. Ho, *Mater. Horiz.* **2017**, *4*, 885–894.
[9] X. Zou, Y. Zhang, *Chem. Soc. Rev.* **2015**, *44*, 5148–5180.
[10] N. V. Lapin, N. Y. D'yankova, *Inorg. Mater.* **2013**, *49*, 975–979.
[11] C. G. Morales-Guio, X. Hu, *Acc. Chem. Res.* **2014**, *47*, 2671–2681.
[12] W.-F. Chen, J. T. Muckerman, E. Fujita, *Chem. Commun.* **2013**, *49*, 8896–8909.

[13] P. Xiao, W. Chen, X. Wang, *Adv. Energy Mater.* **2015**, *5*, 1500985.
[14] I. C. Man, H.-Y. Su, F. Calle-Vallejo, H. A. Hansen, J. I. Martínez, N. G. Inoglu, J. Kitchin, T. F. Jaramillo, J. K. Nørskov, J. Rossmeisl, *ChemCatChem* **2011**, *3*, 1159 – 1165.
[15] H. Wu, T. Yang, Y. Du, L. Shen, G. W. Ho, *Adv. Mater.* **2018**, *30*, 1804341.
[16] X. Long, J. Li, S. Xiao, K. Yan, Z. Wang, H. Chen, S. Yang, *Angew. Chem. Int. Ed.* **2014**, *53*, 7584 – 7588; *Angew. Chem.* **2014**, *126*, 7714 – 7718.
[17] J. Wang, C. F. Tan, T. Zhu, G. W. Ho, *Angew. Chem. Int. Ed.* **2016**, *55*, 10326 – 10330; *Angew. Chem.* **2016**, *128*, 10482 – 10486.
[18] D. A. Lutterman, Y. Surendranath, D. G. Nocera, *J. Am. Chem. Soc.* **2009**, *131*, 3838 – 3839.
[19] K. Xu, P. Chen, X. Li, Y. Tong, H. Ding, X. Wu, W. Chu, Z. Peng, C. Wu, Y. Xie, *J. Am. Chem. Soc.* **2015**, *137*, 4119 – 4125.
[20] M. Ledendecker, S. Krickcalderõn, C. Papp, H. P. Steinrück, M. Antonietti, M. Shalom, *Angew. Chem. Int. Ed.* **2015**, *54*, 12361 – 12365; *Angew. Chem.* **2015**, *127*, 12538 – 12542.
[21] X. Ma, Y. Chang, Z. Zhang, J. Tang, *J. Mater. Chem. A* **2017**, *5*, 2100 – 2106.
[22] H. Wu, X. Lu, G. Zheng, G. W. Ho, *Adv. Energy Mater.* **2018**, *8*, 1702704.
[23] M. Kuang, P. Han, Q. Wang, J. Li, G. Zheng, *Adv. Funct. Mater.* **2016**, *26*, 8555 – 8561.
[24] C. Xiao, Y. Li, X. Lu, C. Zhao, *Adv. Funct. Mater.* **2016**, *26*, 3515 – 3523.
[25] H. Wang, H.-W. Lee, Y. Deng, Z. Lu, P.-C. Hsu, Y. Liu, D. Lin, Y. Cui, *Nat. Commun.* **2015**, *6*, 7261.
[26] J. G. McAlpin, T. A. Stich, W. H. Casey, R. D. Britt, *Coord. Chem. Rev.* **2012**, *256*, 2445 – 2452.
[27] X. Zou, X. Huang, A. Goswami, R. Silva, B. R. Sathe, E. Mikmeková, T. Asefa, *Angew. Chem. Int. Ed.* **2014**, *53*, 4372 – 4376; *Angew. Chem.* **2014**, *126*, 4461 – 4465.
[28] L. Pan, J. H. Kim, M. T. Mayer, M.-K. Son, A. Ummadisingu, J. S. Lee, A. Hagfeldt, J. Luo, M. Grätzel, *Nat. Catal.* **2018**, *1*, 412 – 420.
[29] P. Muthukumar, V. V. Kumar, G. R. K. Reddy, P. S. Kumar, S. P. Anthony, *Catal. Sci. Technol.* **2018**, *8*, 1414 – 1422.
[30] X. Liu, S. Cui, Z. Sun, P. Du, *Chem. Commun.* **2015**, *51*, 12954 – 12957.
[31] B. Kumar, S. Saha, K. Ojha, A. K. Ganguli, *Mater. Res. Bull.* **2015**, *64*, 283 – 287.
[32] H. Xu, J. X. Feng, Y. X. Tong, G. R. Li, *ACS Catal.* **2017**, *7*, 986 – 991.
[33] B. Kumar, S. Saha, A. Ganguly, A. K. Ganguli, *RSC Adv.* **2014**, *4*, 12043 – 12049.
[34] Y. Deng, A. D. Handoko, Y. Du, S. Xi, B. S. Yeo, *ACS Catal.* **2016**, *6*, 2473 – 2481.
[35] Y. Wang, J. Ghanbaja, S. Bruyère, F. Soldera, D. Horwat, F. Mücklich, J. F. Pierson, *Sci. Rep.* **2017**, *7*, 2 – 10.
[36] S. Li, Z. H. Ge, B. P. Zhang, Y. Yao, H. C. Wang, J. Yang, Y. Li, C. Gao, Y. H. Lin, *Appl. Surf. Sci.* **2016**, *384*, 272 – 278.
[37] M. Kuang, T. T. Li, H. Chen, S. M. Zhang, L. L. Zhang, Y. X. Zhang, *Nanotechnology* **2015**, *26*, 304002.
[38] A. Bin Yousaf, M. Imran, S. J. Zaidi, P. Kasak, *Sci. Rep.* **2017**, *7*, 1 – 10.
[39] P. Liu, Z. Li, W. Cai, M. Fang, X. Luo, *RSC Adv.* **2011**, *1*, 847 – 851.
[40] H. Vogt, *J. Electrochem. Soc.* **1990**, *137*, 1179.

Manuscript received: January 11, 2019
Revised manuscript received: February 6, 2019
Accepted manuscript online: February 7, 2019
Version of record online: March 3, 2019

